THE JOURNAL OF PHYSICAL CHEMISTRY C

pubs.acs.org/JPCC Article

Photo-Induced State Shifting in 1D Semiconductor Quantum Wires

William M. Sanderson, Joshua Schrier, and Richard A. Loomis*

Cite This: J. Phys. Chem. C 2020, 124, 16702−16713 Read Online

ACCESS | Metrics & More | Article Recommendations | Supporting Information

ABSTRACT: We report on the time-dependent, energetic shifting of quantum-confinement states within photoexcited CdTe quantum wires that were identified by using transient absorption (TA) spectroscopy. The initial photoexcitation promotes an electron to states in the conduction band (CB) and generates a hole in the valence band (VB), and the changes in carrier densities give rise to quantum-state renormalization (QSR). This mechanism is akin to the generation of electron and hole polarons that alter the effective masses of the states in the CB and VB that are probed in the TA experiments. Since the energies of the quantum-confinement states are inversely proportional to the effective mass of the carrier, the states undergo QSR that evolves as the carriers relax to the band edge. A simple model is presented which separates the bleach and induced-absorption signals associated with QSR in the TA data from additional bleach signals attributed to the occupancy of carriers in the shifted states. The states are observed to shift independently with time as the carriers relax. The lowest-energy occupancy feature for the CdTe quantum wires shifts from −25 to +3 meV within 600 fs and then to −17 meV on longer time scales after excitation. The Stokes shift of the photoluminescence of the CdTe quantum wires is dominated by the long-time scale QSR of the band-edge states. QSR is likely prominent in other direct-gap semiconductor nanoparticles, especially those with a significant Stokes shift of the photoluminescence from the absorption band-gap transitions.

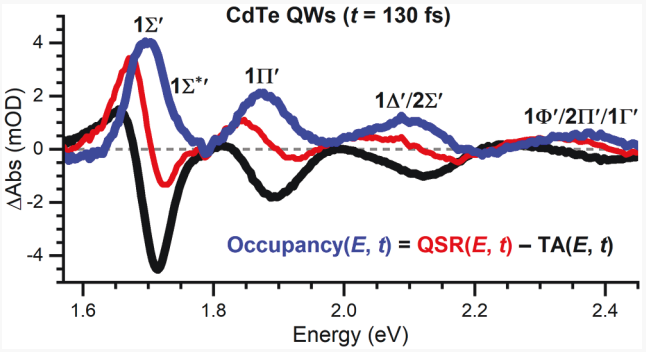

INTRODUCTION

The utilities of semiconductor nanoparticles (NPs) are expanding due to the ability to tune the energies of their electronic states and emission through size control, the sensitivity of their emission efficiency on their environments, and improved synthetic and postsynthetic surface-passivation strategies. An absorption event in a semiconductor NP promotes an electron to the conduction band (CB) and forms a hole, or an electron-deficient region, in the valence band (VB). If the excitation is well above the band gap energy of the NP, the photogenerated electrons and holes can relax from one quantum-confinement state to the next until they occupy the lowest-energy states, near the band edge. The relaxation dynamics of photoexcited electrons and holes within NPs depend on many factors, including size and dimensionality of the NP, efficiency for coupling to phonons, carrier−carrier interactions, ligand coverage, trap densities in the CB and VB, and temperature.[1−5] As these dynamics occur on ultrafast time scales, the specifics and roles of these processes are difficult to characterize. Even under low excitation-fluence conditions, where single electron/hole pairs are generated and probed, the relaxation dynamics of the carriers spectroscopically probed can be complicated due in part to the energetic shifting of the states probed as a function of time after photoexcitation. The absorption of a photon by a semiconductor results in a change in the electron density that perturbs the energetics of the states[6] accessed by the carriers, especially in semiconductor NPs, where there are discrete quantum-confinement states that are highly sensitive to the local environment.

The concept of electron rearrangement in molecules and semiconductors is widely accepted, but it is often not considered in electronic spectroscopy measurements due to the small energetic changes of the states accessed relative to the electronic transition energies. To illustrate the premise for this photogenerated energetic shifting, consider a heteronuclear diatomic, AB, and the molecular orbital (m.o.) diagram illustrated in Figure 1a. An absorption of a photon with energy E_1 promptly promotes an electron from the occupied σ_{AB} m.o. to the unoccupied σ^*_{AB} m.o., assuming it is an allowed transition. After photoexcitation, electron rearrangement relaxes the σ_{AB} and σ^*_{AB} states closer in energy to each other, and the bond lengths of the excited AB molecule adjust to the new bonding.[6] In a pump−probe experiment, a second photon that is delayed in time from the first would be absorbed

Received: May 26, 2020
Revised: June 30, 2020
Published: July 6, 2020

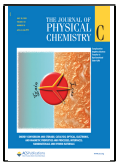

https://dx.doi.org/10.1021/acs.jpcc.0c04755
J. Phys. Chem. C 2020, 124, 16702−16713

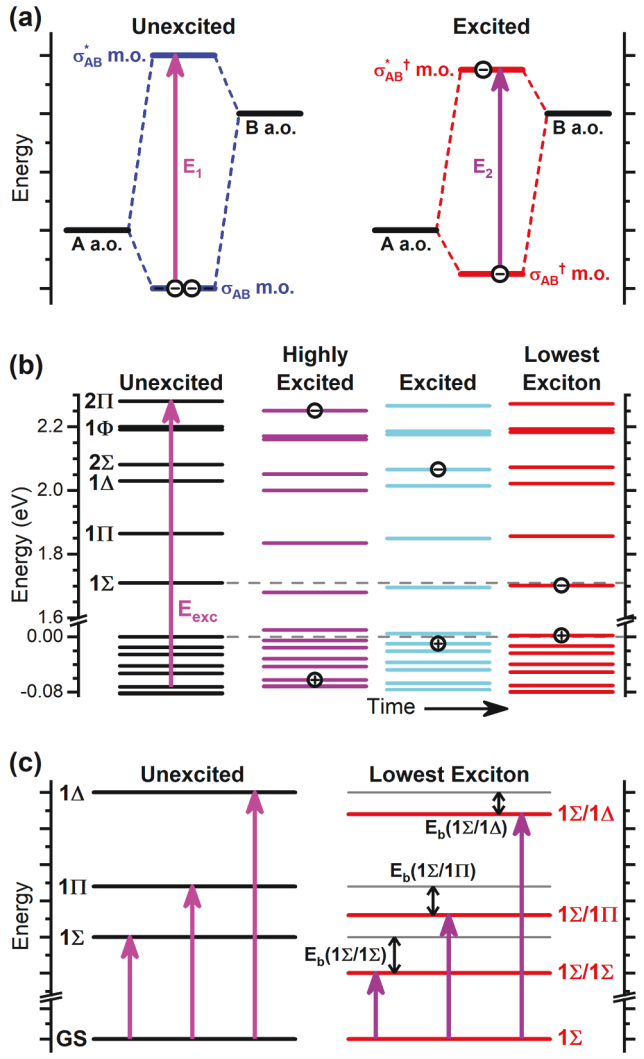

Figure 1. Energetic shifting of states and transitions induced by photoexcitation. (a) Cartoon of a molecular orbital (m.o.) energy diagram for bonding in a heteronuclear diatomic, AB, formed by combining the A and B atomic orbitals (a.o.s). Photoexcitation results in electronic rearrangement, and the energy between the σ_{AB} and σ^*_{AB} m.o. is reduced. (b) The quantum-confinement states of the unexcited CdTe QWs (black) would contribute to a steady-state absorption spectrum. The states in the CB are labeled. Photoexcitation causes a QSR of the states in the VB and CB to higher and lower energies (purple). The QSR lessens as the carriers relax to the lowest exciton states (red), from where the electron and hole can radiatively recombine. (c) The QW excitonic levels that can be accessed in an absorption experiment are shown (left). Features associated with transitions to biexciton levels (right) are often identified in TA experiments. The biexciton levels shown are for the initial electron/hole pair relaxed to the 1Σ state, and the second pair in the 1Σ, 1Π, or 1Δstate. The biexciton binding energies, E_b, are shown.

at a lower-energy, E_2, than E_1 even though the transition is between the same two m.o.s.

The quantum-confinement states of a semiconductor NP accessed with electronic excitation are dictated by the dimensionality of the NP, the local environments of the NP, and the properties of the VB and CB of the unexcited NP, including the effective masses of the carriers. In this article, we report on time-resolved, transient absorption (TA) spectroscopy experiments aimed at probing the shifting of the quantum-confinement states in CdTe quantum wires (QWs). A schematic of the states associated with an unexcited QW is shown as black on the left in Figure 1b. The states in the CB are labeled using the notation appropriate for one-dimensional (1D) QWs with cylindrical symmetry. The absorption of a photon with energy in excess of the band gap, E_{exc}, would promote the electron and hole into excited quantum-confinement states. The change in the electron density within the QW would result in an energetic shifting of the states (highly excited; purple) that would be detected in the probe spectrum acquired in a TA measurement. This energetic shifting of the quantum-confinements states is referred to as quantum-state renormalization (QSR). As the carriers energetically relax through the intermediate states (excited; cyan) to the lowest-energy exciton states near the band edge (lowest exciton; red), the electron density and QSR continuously change. As will be shown, the amount of QSR depends on the energies of and states occupied by the electrons and holes. As a result, the QSR and transition energies probed in a TA spectroscopy experiment shift as a function of time after excitation as the carriers relax to the band edge. Even under low excitation fluences, a single electron/hole pair in a QW would radiatively recombine from states that are energetically shifted by QSR, and this energy difference gives rise to the Stokes shift of the photoluminescence (PL) spectrum from the absorption band edge feature.

This concept of QSR is not necessarily new, as it is akin to the formation of polarons in a semiconductor,[7−9] but it is rarely considered when interpreting TA spectral data collected on NP samples. After a photoexcitation event and the promotion of an electron to the CB and the generation of a hole in the VB in a spatial region within a semiconductor, the surrounding ions within the semiconductor interact through Coulombic forces with the electron and hole; the cations (anions) will be slightly attracted to the excited electron (hole). The ions in the semiconductor lattice adjust their positions slightly, balancing their interactions with the charge carriers and the bonding forces that hold the ions in their equilibrium positions. The change in lattice structure results in a polarization locally centered at the positions of the carriers but that can extend well beyond the size of the electrons, holes, or excitons. The term polaron describes the interacting charge carriers and lattice polarization.[7−9] The characterization of polarons in bulk CdTe and CdSe initially involved the direct probing of the transitions between Landau levels in varying magnetic fields.[10−13] More recently, polarons in NPs[14−16] and their role in charge transfer between them[17] have also been reported. The impact of photoexcitation and the formation of polarons on the quantum-confinement states in NPs, i.e., QSR, has yet to be explored, and is presented herein for CdTe QWs.

The energies of the quantum-confinement states in a semiconductor NP are typically approximated using effective-mass models, and their energies in the CB and VB are inversely proportional to the effective masses of the electrons and holes. The effective masses of the carriers and the quantum-confinement states in an unexcited NP that would be probed in a low-fluence, steady-state absorption experiments are dictated by the ground-state electronic configuration of and interactions within the NP. After photoexcitation, the formation of polarons perturbs the shapes of the CB and VB, and the effective masses of the carriers become larger.[7−9,18−20] As a result, each quantum-confinement state will experience a QSR that depends on the altered effective

https://dx.doi.org/10.1021/acs.jpcc.0c04755
J. Phys. Chem. C 2020, 124, 16702−16713

masses of the carriers, the wave functions of that state,[20,21] and the dimensionality and sizes of the NPs.[19−22] Polaron models indicate that a smaller confinement dimension will result in a larger change in the carrier effective masses with the formation of a polaron. A smaller confinement dimension would correspondingly result in a larger QSR, and these energetic shifts may be on the order of the exciton stabilization energy of the electron and hole.[21] Polaron models also predict larger perturbations for semiconductor NPs with confinement in two dimensions (2D), i.e., for QWs, and in one dimension, i.e., for quantum wells or quantum platelets, than for confinement in three dimensions (3D), i.e., for quantum dots (QDs).[19−21] As a result, the resultant effects of QSR may be largest in 1D QWs.

TA spectroscopy experiments are commonly performed on semiconductor NPs to characterize the relaxation dynamics of charge carriers or the energetic changes of the quantum-confinement states or interactions within the NPs caused by photoexcitation. In a steady-state absorption experiment performed using extremely low excitation fluences, where less than one photon would be absorbed by any single NP, only transitions to the single exciton levels would be present in the absorption spectrum. These transitions for a QW are illustrated on the left side of Figure 1c. Multiphoton excitation of a semiconductor NP, whether a result of using high excitation fluences or performing two-pulse, pump−probe TA experiments, could result in the generation of multiple electron−hole pairs in a NP. Under these conditions, two electron−hole pairs can be stabilized as biexcitons through electrostatic and exchange interactions.[1,3,23−44] In principle, biexcitons can be stabilized with either exciton in the ground or an excited exciton level, which have hydrogenic-like wave functions, and with the electrons and holes in any of the quantum-confinement states,[45] e.g., the 1Σ, 1Π, 1Δ, ... states for QWs. A schematic of the bound biexciton levels associated with the lowest exciton levels for both the electron and hole 1Σ quantum-confinement states and the carriers in the second exciton in the different states are shown as red levels on the right side of Figure 1c. The binding energies for each of these biexciton levels would be dissimilar, but if the biexcitons are bound, the binding energies, E_b, would be positive, and the transitions accessed in a spectrum would appear to lower energies then the single-exciton transitions by an amount E_b. Signals associated with transitions accessing biexcitons would appear as positive or induced-absorption features in a TA spectrum.

Historically, induced-absorption features observed to lower energies than the band-edge exciton feature in TA data collected on samples of QDs[1,3,27−35] and QWs[36−41] are often assigned as biexciton transitions. As expected for the stabilization of biexcitons, the intensities of these features often follow a quadratic dependence on excitation fluence. Due to the translational degrees of freedom available for charge carriers and excitons in QWs, quantum wells, and bulk, it seems unlikely that biexcitons could be stabilized at room temperature and under low-excitation fluence conditions; two excitons would have to encounter each other, transfer energy and momentum to the semiconductor or another carrier particle, and remain bound despite the thermal energy present. The results from experiments[26] and theory[25,46] indicate it is also possible for biexciton transitions to appear to higher energies than the lowest-energy exciton feature. Such a shift would likely occur in small NPs, where the electrons and holes are forced to overlap each other and the repulsive Coulombic forces between like charges dominate over the attractive forces. Although there are still two electron−hole pairs interacting, the excitons would be only bound to each other in these small NPs due to the spatial confinement of the NP.

Herein, we present the results of TA spectroscopy experiments performed on CdTe QWs aimed at identifying the energetic changes incurred during photoexcitation and throughout the state-to-state relaxation of the charge carriers to the band-edge states after excitation. The TA data collected are typical of those collected on most semiconductor NPs and contain overlapping induced-absorption and bleach signals throughout the spectral region probed.[1,3−5,32,33,43,44,47−52] As we will show, some of these signals can be associated with QSR induced by the photoexcitation. The QSR gives rise to an induced-absorption signal to lower energies than the lowest-energy exciton feature in the steady-state absorption spectrum that is often associated with biexciton transitions. Experiments were performed using varying excitation fluences and with two different excitation energies, and the relative contribution of this induced-absorption feature remains constant at fluences <20 $\mu J\ cm^{-2}\ pulse^{-1}$. Furthermore, the energy and shape of this feature is nearly identical to the steady-state PL spectrum of the CdTe QWs. Since the PL results from the radiative recombination of single electron−hole pairs, the induced-absorption feature is also attributed to single excitons. There is no evidence for contributions in the PL spectrum or the TA data from biexciton transitions. Once the QSR is accounted for, the state-to-state time-dependent shifting of the different spectral features is identified, and the relaxation of the carriers after initial excitation down to the band edge states can be easily identified. While this work focuses on the QSR in CdTe QWs and a simple model for analyzing TA data, the state-to-state intraband relaxation dynamics of the charge carriers characterized using the QSR model were recently reported in ref 53.

EXPERIMENTAL METHODS

CdTe QW Sample. The colloidal sample of CdTe QWs was synthesized using the solution-liquid−solid method.[54,55] Specifically, the CdTe QWs were grown using 9.1 nm-diameter bismuth nanoparticles at 250 °C in the presence of di-*n*-octylphosphine (0.14 mol %). Cd(di-*n*-octylphosphinate)$_2$ and tri-*n*-octylphosphine telluride (TOPTe, 0.025 mmol/g) were used as the Cd and Te precursors with a Cd/Te precursor mole ratio of 2.8. After synthesis, the CdTe QWs were stored in a N_2-purged glovebox until the steady-state and time-resolved spectroscopy experiments were performed. See Figure S1 for typical low- and high-resolution TEM images of the CdTe QWs. High-resolution TEM analysis of the CdTe QWs indicated they had an admixture of wurtzite and zinc blende crystal phases with nearly equal contributions. The mean diameter of the CdTe QWs was measured to be 7.5(9) nm with typical lengths between 1 and 10 μm. The CdTe QWs were used without additional postsynthesis treatment.[55]

Steady-State Spectroscopy. The premise for the QSR model is to spectroscopically identify the quantum-confinement states of the unexcited and excited NP sample and the occupancy of the states of the excited NP with time. An absorption spectrum of the NP sample, $Abs_{SS}(E)$, is utilized in the model to account for the induced-absorption and bleach features associated with QSR. It is imperative that a "clean" absorption spectrum of only the NP sample is used, or the

https://dx.doi.org/10.1021/acs.jpcc.0c04755
J. Phys. Chem. C 2020, 124, 16702−16713

QSR cannot be properly fit and accounted for. As a result, particular care must be taken when recording the $Abs_{SS}(E)$ spectrum, and two possible contributions to the spectra of the CdTe QW samples were considered. First, the physical dimensions of each CdTe QW sample were characterized using TEM, and the size distributions were measured. If a sample contains widely varying diameter distributions, the quantum-confinement and shifting due to QSR may be inhomogeneous, which is beyond the scope of this model. Second, contributions from Rayleigh scattering in the absorption spectrum were removed. Because of the large volumes of the individual semiconductor QWs, especially in comparison to those of molecules or semiconductor QDs, and the tendency for QWs to bundle, steady-state absorption spectra of QWs often contain contributions from scattering and are more properly referred to as extinction spectra.

The extinction spectra of the CdTe QWs were collected using a commercial absorption spectrometer coupled with an integration sphere to collect forward-facing scattered light. The spectra were acquired using a resolution of 3 nm, step sizes of 1 nm, and an integration time of 0.4 s. The CdTe QWs were diluted in dry toluene, and the concentrations were kept low, resulting in extinction values <0.2 throughout the probe spectral region, to minimize nonlinearities and the tendency for clustering of the QWs. Even then, the spectra contained small contributions from scattering, as evidenced by a nonzero background signal below the lowest-energy feature, the 1Σ feature for the CdTe QWs, that increases with photon energy, E, see Figure S2. In order to remove this additional scattering contribution, the extinction spectra were recorded over broad energy or wavelength regions so that regions lying energetically well below the band gap of the material were collected. At these low energies, the only losses should be from scattering, which has a dependence on photon energy, E_{ph}, given by

$$\text{Scattering}\ (\lambda) = y_0 + AE_{ph}^{\ 4} \tag{1}$$

where y_0 is an instrumental baseline offset and A is a proportionality constant related to the material and volume of the NPs. Each extinction spectrum was fit to the scattering equation for energies below the band gap, and the obtained scattering component was subtracted from the entire spectrum to obtain a "clean" $Abs_{SS}(E)$ spectrum of the CdTe QWs. The peaks in each $Abs_{SS}(E)$ spectrum were identified by taking the second-derivative of the spectrum; see Supporting Information.

A commercial spectrofluorometer was used to record the PL spectra ($PL(E)$) and to measure the PL quantum yield (Φ_{PL}) of the CdTe QWs with excitation at 2.76 eV. A spectral resolution of 3 nm and an integration time of 0.5 s were used during the $PL(E)$ measurements. The peak in each $PL(E)$ is Stokes shifted by ∼17 meV below the peak of the lowest-energy absorption feature for these CdTe QWs, Figure S4. The PL of these CdTe QWs is weak, and an ensemble Φ_{PL} of just 0.20(3) % was measured using 2.76 eV excitation.

Transient Absorption Spectroscopy. The TA data, $\Delta Abs_{TA}(E, t)$, of the CdTe QWs were collected using a commercial TA spectrometer. Femtosecond excitation and probe pulses were produced using a 1 kHz regenerative amplifier system with an optical parametric amplifier using fourth harmonic generation of the idler. Excitation pulses centered at E_{exc} = 2.75 or 2.26 eV were used with a probe spectrum spanning from ∼1.51 to ∼3.10 eV. The temporal response of the TA measurements was measured to be ∼200 fs based on optical Kerr-effect signals induced in a quartz coverslip placed at the position of the sample. A sealed 0.2 cm quartz cuvette was used for the TA experiments, and the extinction of the CdTe QWs was kept <0.2 at the excitation energy, 2.75 eV. The samples were stirred using a magnetic stir bar. Five consecutive TA data sets were collected and then averaged when using low excitation fluences. The average TA data sets were chirp-corrected. A low excitation fluence of 9.7 $\mu J\ cm^{-2}\ pulse^{-1}$ was used to minimize contributions from multiphoton excitation, carrier−carrier interactions, and nonlinear effects. Experiments were performed using a range of excitation fluences to verify negligible signals associated with multiphoton excitation were measurable when using 9.7 $\mu J\ cm^{-2}\ pulse^{-1}$, Figure S6.

CALCULATIONS

The transitions contributing to each absorption feature are proposed through comparison with a spectrum calculated using the method of local density approximation with band-corrected pseudopotential (LDA+C) for 7.3 nm diameter CdTe QWs, performed in a similar manner as reported previously.[56,57]

Quantum-Confinement States. Electronic structure calculations of the CdTe nanowires were performed using the LDA+C method described in our previous work.[56,57] This consists of two stages. First, a set of standard self-consistent planewave nonlocal pseudopotential local density approximation (LDA) calculations were performed on bulk zinc-blende CdTe and pseudohydrogen passivated surfaces, using PEtot.[58] A 35 Ry planewave energy cutoff was used, and spin−orbit coupling was ignored for the valence bands. Since LDA underestimates both the electron band gap and the electron effective mass, the pseudopotentials are perturbed in the LDA +C method so that their use in a nonself-consistent calculation results in the bands having the correct effective masses. An additive constant shift in energy, specifically 0.440 eV, was added to the calculated band gap to yield the experimental bulk band gap.[56,57] From the self-consistent bulk and surface results obtained with the standard pseudopotential, we then extracted atom-centered electron density motifs describing each environment (e.g., Cd completely surrounded by Te atoms, Cd with three Te and one pseudohydrogen, etc.); these were then assembled to construct an approximate charge density of the nanowire.[56,59] Using this reconstructed density and the band-corrected pseudopotentials, a linear-scaling nonself consistent folded spectrum equation was solved to determine 15 conduction band states, ϕ_c, and 100 valence band states, ϕ_v, nearest to the band gap using PEscan.[60] To sample the Brillouin zone of the nanowire, we calculated 5 k-points along the c axis and then linearly interpolated the energies and transition dipole matrix elements for 27 intermediate points.

Transition Energies and Probabilities. The imaginary part of the dielectric function is proportional to the optical absorption spectrum to within a volume factor, and it was computed by summing the momentum operator integrals over all k-points (k), the conduction band ("electron") indices (c), and the valence band ("hole") indices (v)[61,62]

$$\epsilon_i(\omega) = \frac{8\pi^2 e^2 \hbar^2}{3m^2(\hbar\omega)^2 V} \sum_k \sum_{c,v} |\langle \phi_c(k)|\hat{p}|\phi_v(k)\rangle|^2 \delta(E_c(k) - E_v(k) - \hbar\omega) \tag{2}$$

https://dx.doi.org/10.1021/acs.jpcc.0c04755
J. Phys. Chem. C 2020, 124, 16702−16713

where *e, m, and V* are the electron charge, electron mass, and volume of the system. The Dirac delta function conserves energy between the electron eigenstate $E_c(k)$ and the sum of the hole eigenstate $E_v(k)$, and the incoming photon energy, $\hbar\omega$. The calculations resulted in a discrete set of transitions, which we broadened with a Gaussian function with a breadth of 20 meV. The transition energies are $E_c(k) - E_v(k)$ and the transition probabilities are the squared momentum matrix elements $|\langle\phi_c|\hat{p}|\phi_v\rangle|^2$. The transitions included in Supporting Information, Table S2 only include the Γ-point transitions (k = 0). The calculated transition energies are slightly higher than the observed absorption features, and they have been shifted by 40 meV to lower energy to better overlap with the lowest-energy, 1Σ, feature centered at 1.703 eV.

There is mixing of the quantum-confinement states in the VB that prohibits identification of their quantum numbers. The states in the CB have larger energy spacings between them, and there is no obvious state mixing. As a result, each feature is labeled using only the quantum numbers of the states in the CB that are accessed. The most intense calculated transitions are plotted as sticks in Figure 2a. The weak feature labeled 1Σ* near 1.78 eV identified in the second derivative analysis of the $Abs_{SS}(E)$ spectrum is not predicted by the calculations. This feature is likely associated with the highest-energy 1Σ transition calculated, which is a transition between an energetically excited hole state and the 1Σ electron state.

RESULTS

Spectroscopy. A typical $Abs_{SS}(E)$ spectrum of the CdTe QWs suspended in dried toluene is plotted in Figure 2a. Four broad, prominent features and one weaker feature, the 1Σ* feature at 1.78 eV, are associated with groups of transitions between quantum-confinement states in the VB and CB. The calculated transitions indicate the breadths of the prominent features are largely dictated by the numerous transitions accessing common states in the CB; the calculated transitions are color coded by the states accessed in the CB, and each feature is labeled by those states.

The TA spectra of the CdTe QWs, $\Delta Abs_{TA}(E, t)$, were recorded using both E_{exc} = 2.75 and 2.26 eV, and the data have similar characteristics. The $\Delta Abs_{TA}(E, t)$ acquired using E_{exc} = 2.75 eV are described here, and the results obtained using E_{exc} = 2.26 eV will be compared below. The $\Delta Abs_{TA}(E, t)$ recorded at most of the time delays, t, are dominated by bleach signals, $\Delta Abs_{TA}(E, t) < 0$, that lie close in energies to the features observed in the $Abs_{SS}(E)$, indicated by vertical dotted lines in Figure 2b. These bleach signals appear promptly with an instrument-limited rise time. All of the bleach features, even those associated with transitions accessing excited quantum-confinement states, e.g., the 1Π, 1Δ/2Σ, and 1Φ/2Π/1Γ features, are measurable for time scales out to ∼1 ns. Intraband relaxation should be complete by this time, and the carrier populations should be in the lowest-energy electron and hole states.[1,3,4,32,33,43,44,47−51,63−76] There are also numerous induced-absorption signals, $\Delta Abs_{TA}(E, t) > 0$, that are noticeable to varying amounts at different t. For instance, there is an induced-absorption feature at energies below the band gap, ∼1.65 eV, at short t; see the t = 0.4 ps spectrum in Figure 2b. At longer t, this signal is no longer present, and an induced-absorption feature grows in at higher energies than the 1Σ feature, as shown in the t = 5.0 ps spectrum in Figure 2b. There are also weaker induced-absorption features at higher

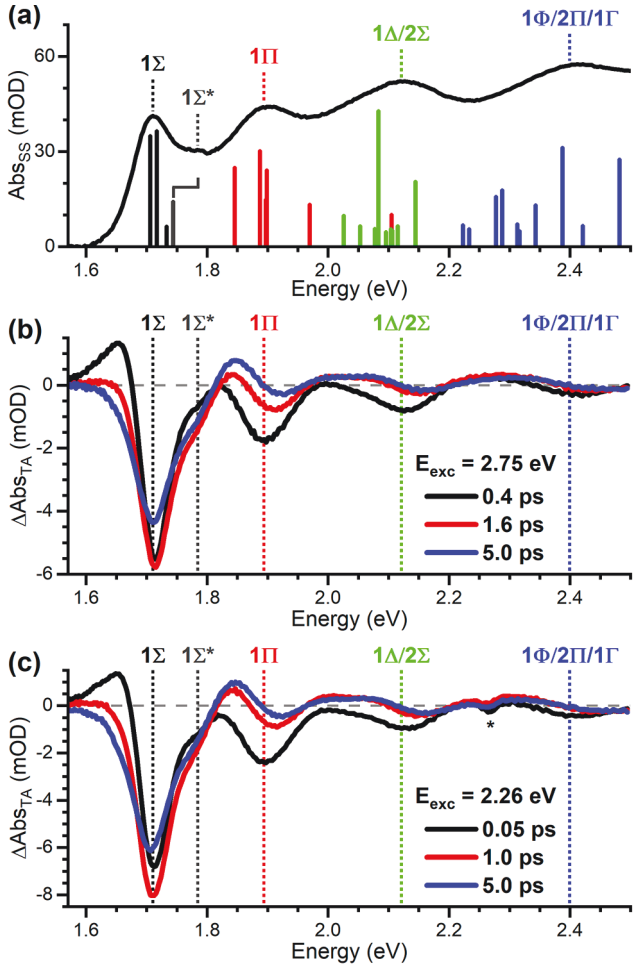

Figure 2. Spectral data of CdTe QWs. (a) Steady-state absorption spectrum of CdTe QWs. The dominant transitions (plotted as sticks) were calculated using LDA+C.[56,57] The labels of the CB states accessed within each feature are included. (b) TA spectra recorded using E_{exc} = 2.75 eV at t = 0.4, 1.6, and 5.0 ps are plotted as black, red, and blue, respectively. (c) TA spectra recorded using E_{exc} = 2.26 eV at t = 0.05, 1.0, and 5.0 ps are plotted as black, red, and blue, respectively. The small dip in the signal marked with an * is due to scattering of E_{exc}. The data in parts a and b were published in a different format in ref 53.

energies, ∼2.05 and ∼2.30 eV, that remain measurable at long t.

The evolution of the bleach and induced-absorption signals with time are not necessarily the same, and the features appear to move with time resulting in complicated temporal profiles within the $\Delta Abs_{TA}(E, t)$ data. The induced-absorption signals in the TA spectra observed just below the band gap are often attributed to BGR,[77−82] Stark shifting of the quantum-confinement states,[1,28,43,49,83] or biexciton states[1,3,25,27−30,32,33,43−45] associated with multiple, interacting electron−hole pairs within each NP. The extremely short lifetimes of the lowest-energy, induced-absorption signals seem consistent with the role of carrier−carrier interactions and efficient Auger relaxation,[52,84−86] which will promptly reduce the carrier densities in the NPs and quench these induced-absorption signals. Even though the TA data were collected using very low excitation fluences, additional TA experiments were performed using higher excitation fluences to identify possible contributions from multicarrier interactions.

https://dx.doi.org/10.1021/acs.jpcc.0c04755
J. Phys. Chem. C 2020, 124, 16702−16713

As these types of higher-order contributions do not scale linearly with excitation fluence, all of the features should not scale together if these contributions are present in the data. No changes in the relative amplitudes of the induced-absorption and bleach features were observed at short t, when carrier−carrier interactions should dominate, with excitation at E_{exc} = 2.75 eV and with fluences <20 μJ cm^{-2} pulse^{-1} (Figure S6a). Changes in the shapes of the TA features were observed in the TA spectra recorded using fluences of 57 μJ cm^{-2} pulse^{-1} and higher. These changes are attributed to contributions from multicarrier interactions, to phonon excitation or warming of the sample as carriers relax, or to carrier trapping that can occur either during intraband relaxation or after they reach the band edge. Only small differences in the temporal profiles of the 1Σ feature are observed when comparing the data measured at fluences of 9.7 and 17.3 μJ cm^{-2} pulse^{-1} (Figure S6b). As a result, none of the signals in the TA data acquired using a fluence of 9.7 μJ cm^{-2} pulse^{-1} are associated with interacting multiple electron−hole pairs, BGR, Stark shifting, or biexciton states. Similar results were obtained for E_{exc} = 2.26 eV, Figure S7. Unless otherwise stated, the TA data presented was collected using fluences of 9.7 and 11.2 μJ cm^{-2} pulse^{-1} for E_{exc} = 2.75 and 2.26 eV, respectively.

QSR Model. Some of the complicated dynamics present in the $\Delta Abs_{TA}(E, t)$ data are due to QSR, and we present a simple model to separate the contributions from QSR and the changing carrier occupancies in the different states. The premise of the QSR model is summarized in Figure 1b and Figure 3 using CdTe QWs as an example. The band diagram

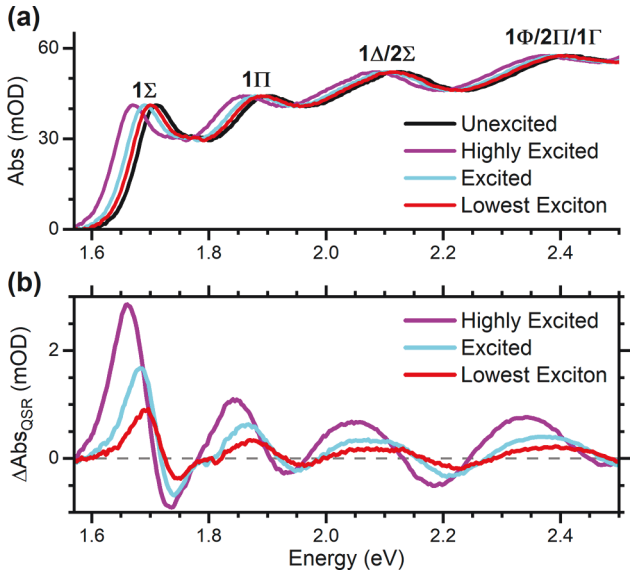

Figure 3. QSR model as applied to CdTe QWs. (a) The QSR results in a shifting of the probe absorption spectra with time. (b) The contributions of QSR in the TA spectra, $\Delta Abs_{QSR}(E, t)$, are obtained by subtracting the steady-state absorption spectrum, $Abs_{SS}(E)$, black in part a, from the probe spectra recorded at the different times, $Abs_{SS}(E - \Delta E_{QSR}(t))$, purple, cyan, and red.

(black; Figure 1b) contains the unperturbed quantum-confinement states accessed in the $Abs_{SS}(E)$ spectrum (black; Figure 3a). The absorption of a photon with E_{exc} that is greater than the band gap, 1.703 eV for these CdTe QWs, generates a highly excited electron−hole pair. The resultant change in electron density and interactions within the QW give rise to QSR of the quantum-confinement states in the CB and VB of the CdTe QW. At this short time, the QSR is the largest, and as illustrated in the purple band diagram, the quantum confinement states in the VB are shifted up to higher energies and those in the CB are shifted down to lower energies. An initial assumption is made in this model that all of the confinement states in the CB shift by the same energy, and those in the VB also shift by the same amount, which may be different than the shift in the CB. The results presented for CdTe QWs indicates this assumption is appropriate for the TA data collected after the carriers have relaxed to the band-edge states, t > 5 ps. Additional independent shifting of the quantum-confinement features at earlier times is revealed once the carrier occupancies in the different states are extracted.

To illustrate the contributions of QSR in the TA data, the optical excitation was assumed to generate arbitrary shifts of −30 meV and +10 meV for the quantum-confinement states in the CB and VB (purple), in Figure 1b. As a result, the instant after excitation, the $\Delta E_{QSR}(t)$ shift would be −40 meV, and a shifted induced-absorption spectrum, $Abs_{SS}(E-\Delta E_{QSR}(t))$, would result (purple; Figure 3a). A little after excitation, the electron and hole would relax toward the band edge, most likely with dissimilar rates, and the $\Delta E_{QSR}(t)$ would decrease with t; ΔE_{QSR}(1 ps) was set to −20 meV (cyan; Figure 1b and Figure 3a). Ultimately, after the IRD of the carriers is complete, the electron and hole would be stabilized in the lowest exciton states (red; Figure 1b). The band gap energy and all of the optical transitions would still be perturbed by QSR, as illustrated with ΔE_{QSR}(5 ps) fixed at −10 meV (red; Figure 3a), and the value of $\Delta E_{QSR}(t)$ would remain constant until the electron and hole either radiatively or nonradiatively recombine.

The changes in the absorption spectra that occur with t after photoexcitation are precisely what is probed in a TA spectroscopy experiment. The effects of QSR will have contributions in the $\Delta Abs_{TA}(E, t)$ resulting in additional increases or decreases in bleaching intensities at different energies that will distort the decay profiles. Examples of QSR contributions, $\Delta Abs_{QSR}(E, t)$, for short-, intermediate-, and long-time delays are plotted in Figure 3b. These model transient spectra were obtained by subtracting the black unperturbed $Abs_{SS}(E)$ spectrum from the purple, cyan, and red $Abs_{SS}(E-\Delta E_{QSR}(t))$ spectra. The shifting of the absorption spectra with t due to QSR directly gives rise to induced-absorption and bleach signals in TA data that span the full spectral region. The method of shifting the $Abs_{SS}(E)$ spectrum has been incorporated previously to interpret $\Delta Abs_{TA}(E, t)$ data collected on CdSe QDs,[34,35] CdSe nanoplatelets,[43] and carbon nanotubes.[87,88] The dynamics observed in those studies were interpreted as being due to the stabilization of biexcitons[34,35,43,87] or Stark shifting[88] associated with multiple interacting carriers, but we suggest they could likely be due to QSR.

The illustration presented above indicates that the relative amplitudes of the features in the $\Delta ABS_{QSR}(E, t)$ spectra depend on $\Delta E_{QSR}(t)$. The overall amplitude of the $\Delta ABS_{QSR}(E, t)$ signal is proportional to the population of electrons and holes in the NPs, which are included as a carrier population coefficient, $C(t)$. The contributions of QSR in experimental TA data are approximated by

https://dx.doi.org/10.1021/acs.jpcc.0c04755
J. Phys. Chem. C 2020, 124, 16702−16713

$$\Delta \mathrm{Abs}_{\mathrm{QSR}}(E, t) = \mathrm{C}(t)[\mathrm{Abs}_{\mathrm{SS}}(E - \Delta \mathrm{E}_{\mathrm{QSR}}(t)) - \mathrm{Abs}_{\mathrm{SS}}(E)] \quad (3)$$

The contributions from QSR in a TA spectrum recorded at each t would ideally be obtained by fitting eq 3 to the TA spectrum, $\Delta \mathrm{Abs}_{\mathrm{TA}}(E, t)$, using $\mathrm{C}(t)$ and $\Delta E_{\mathrm{QSR}}(t)$ as fitting parameters. It can be challenging, however, to fit and determine $\mathrm{C}(t)$ and $\Delta E_{\mathrm{QSR}}(t)$ over all t. For instance, it is necessary to avoid the inappropriate fitting of contributions from bleach signals in the TA data associated with carrier occupancies. Instead, it is appropriate to fit the higher-energy region of the TA spectra at long t, when the high-energy states are no longer occupied. For the CdTe QWs, the energy region and time windows appropriate for the QSR fitting were determined by normalizing the TA spectra to the same ΔAbs value at E = 2.05 eV. In these CdTe QW TA data, the relative amplitudes of the induced-absorption and bleach features in the energy region 1.8 eV ≤ E ≤ 2.5 eV remained the same for 5 ps ≤ t ≤ 300 ps, which verifies there were no bleach signals associated with carrier occupancies. The fit for t = 35 ps and $\mathrm{E}_{\mathrm{exc}}$ = 2.75 eV is included in Figure 4a, and $\Delta E_{\mathrm{QSR}}(35\ \mathrm{ps})$ = 13.0(4) meV was obtained. There are only differences between the $\Delta \mathrm{Abs}_{\mathrm{TA}}(E, 35\ \mathrm{ps})$ and $\Delta \mathrm{Abs}_{\mathrm{QSR}}(E, 35\ \mathrm{ps})$ spectra at E < 1.8 eV, where occupancy signals contribute. Examples of the fits over this energy region of the TA spectrum for four different times are included in Figure S8. A mean value of $\Delta E_{\mathrm{QSR}}(t)$ = 13.0(1.0) meV was determined for the $\Delta \mathrm{Abs}_{\mathrm{TA}}(E, t)$ data collected with $\mathrm{E}_{\mathrm{exc}}$ = 2.75 eV and t ≥ 5 ps. The C(t) values are plotted in Figure 4b (open circles) for this time window. The QSR signals remained in the TA data for t > 300 ps, but the signals across the 1.8 eV ≤ E ≤ 2.5 eV region were too low to obtain reliable fits using two parameters. Since there appeared to be no additional shifting of the features in the $\Delta \mathrm{Abs}_{\mathrm{TA}}(E, t)$ data at these long t, $\Delta E_{\mathrm{QSR}}(t > 300\ \mathrm{ps})$ was fixed to 13.0 meV, and the $\mathrm{C}(t)$ values were obtained using it as the sole fitting parameter in eq 3. These $\mathrm{C}(t)$ values are also plotted in Figure 4b. Similar analyses were undertaken on the data collected using $\mathrm{E}_{\mathrm{exc}}$ = 2.26 eV, included in Supporting Information. A QSR shift of $\Delta E_{\mathrm{QSR}}(t)$ = 12(2) meV was obtained, and it is the same within error as obtained using $\mathrm{E}_{\mathrm{exc}}$ = 2.75 eV, $\Delta E_{\mathrm{QSR}}(t)$ = 13.0(1.0) meV.

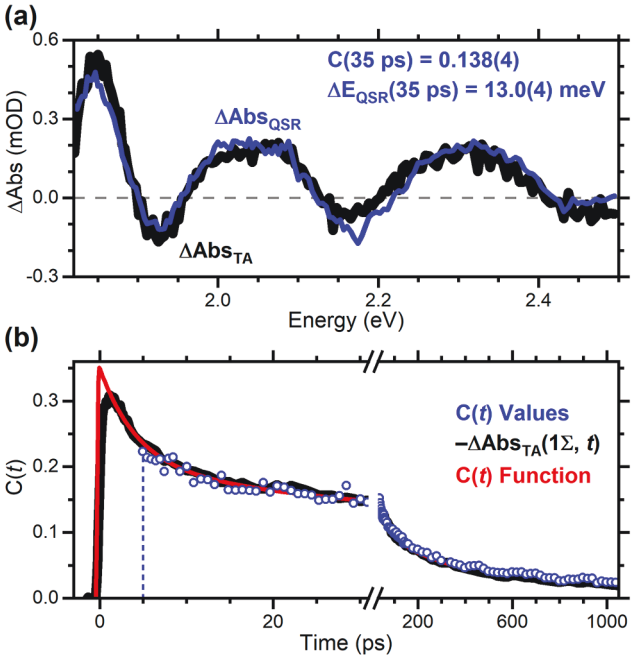

Figure 4. Schematic depicting how the $\mathrm{C}(t)$ and $\Delta E_{\mathrm{QSR}}(t)$ values are obtained using the TA data collected. (a) The QSR spectrum, $\Delta \mathrm{Abs}_{\mathrm{QSR}}(E, 35\ \mathrm{ps})$, (blue) was fit to the TA spectrum (black) recorded at t = 35 ps using $\mathrm{C}(t)$ and $\Delta E_{\mathrm{QSR}}(t)$ as fitting parameters with values shown. (b) The $\mathrm{C}(t)$ factors obtained by fitting the TA spectra for $t \geq 5$ ps (blue, open circles) were then used to scale the total carrier population decay profile (red), $\mathrm{C}(t)$, over all t. The fitting for t > 300 ps was performed using a fixed $\Delta E_{\mathrm{QSR}}(t)$ = 13.0 meV and $\mathrm{C}(t)$ as the sole parameter. For shorter times, t < 5 ps, the negative of the TA 1Σ bleach profile, $-\Delta \mathrm{Abs}_{\mathrm{TA}}(1\Sigma, t)$, (black) was fit to a sum of exponential decays. The fit parameters were then used to extrapolate $\mathrm{C}(t)$ to shorter t, where an instrument-limited rise time, 200 fs, was included.

In order to extrapolate the $\mathrm{C}(t)$ factors to shorter times, the 1Σ bleach was fit to an exponential growth and a sum of four exponential decays convoluted with a 200 fs Gaussian instrument response function using the equation

$$\Delta Abs_{1\Sigma}(t) = \mathrm{IRF} \otimes \left[\sum_{i=1}^{4} (A_i \exp(-t/\tau_i)) - A_{\mathrm{rise}} \exp(-t/\tau_{\mathrm{rise}}) \right] \quad (4)$$

The fits for $\mathrm{E}_{\mathrm{exc}}$ = 2.75 and 2.26 eV are included in Figures S13 and S14, and the obtained parameters are listed in Tables S3 and S4. The growth of the 1Σ TA profile is complicated due to overlapping bleach and induced-absorption signals, and there are contributions that appear immediately and that grow in as the excited carriers relax to the 1Σ quantum-confinement states. As a result, the rise of the 1Σ TA profile does not track with the total population of the carriers that was in the QWs. Instead, the rise of the total population of carriers in the QWs was dictated by the excitation pulse. Consequently, the exponential decays obtained in the fitting (Table S3) were convoluted with an instrument-limited rise time to obtain a $C(t)$ function that represented the population of the charge carriers over the duration of the TA experiments (red; Figure 4b). Ultrafast dynamics that deplete either the electron or hole populations on time scales <5 ps may lead to an underestimation of the $C(t)$ values in this temporal window using this extrapolation method.

The $C(t)$ function and $\Delta E_{\mathrm{QSR}}(t)$ = 13.0 meV was used to obtain the $\Delta \mathrm{Abs}_{\mathrm{QSR}}(E, t)$ for the CdTe QWs overall the full temporal window and collected using $\mathrm{E}_{\mathrm{exc}}$ = 2.75 and 2.26 eV. The $\Delta \mathrm{Abs}_{\mathrm{QSR}}(E, t)$ and $\Delta \mathrm{Abs}_{\mathrm{TA}}(E, t)$ spectra for t = 35 ps and 130 fs with $\mathrm{E}_{\mathrm{exc}}$ = 2.75 eV are plotted in Figure 5a,c as blue and black, respectively. At longer t, e.g., t = 35 ps, the prominent differences between these spectra are in the low energy region, and these differences are attributed to carriers occupying the lowest-energy states near the band edge. In contrast, there are

https://dx.doi.org/10.1021/acs.jpcc.0c04755
J. Phys. Chem. C 2020, 124, 16702−16713

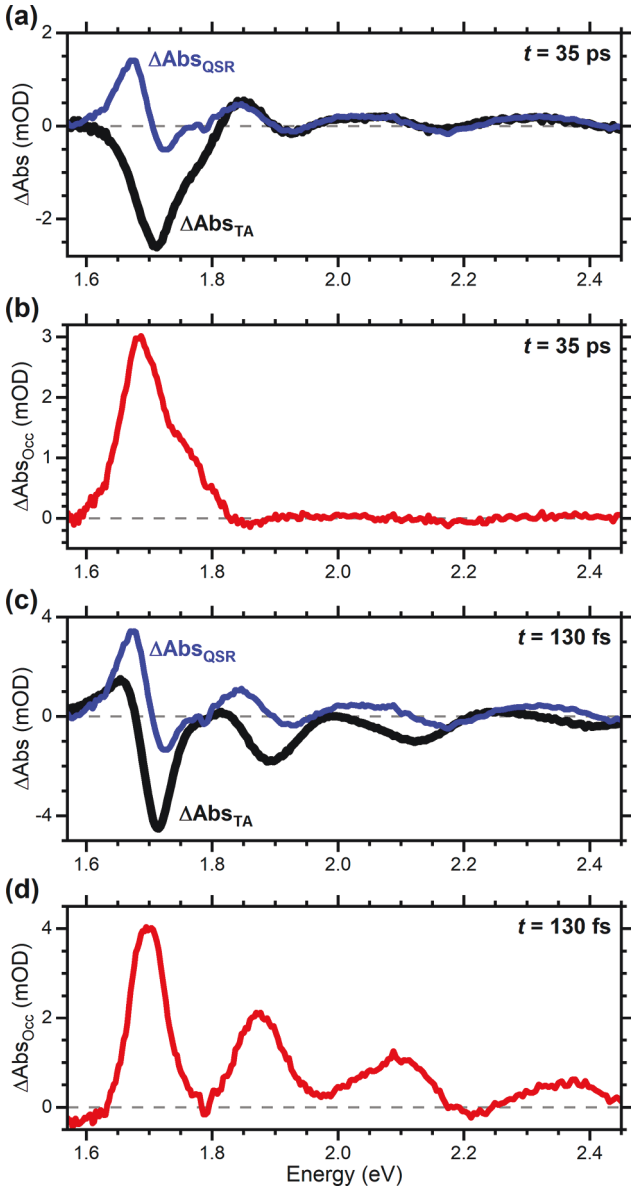

Figure 5. Determination of the occupancy data, $\Delta Abs_{Occ}(E, t)$, using the QSR model. The ΔAbs_{TA} (black) and ΔAbs_{QSR} (blue) spectra of the CdTe QWs at t = 35 ps and 130 fs obtained with E_{exc} = 2.75 eV are plotted (a and c). The difference between the ΔAbs_{QSR} and ΔAbs_{TA} spectra at each t yields the corresponding $\Delta Abs_{Occ}(E, t)$ spectrum (b and d).

differences between these spectra throughout the entire spectral region at short t, e.g., t = 130 fs. These differences are attributed to bleach signals associated with carriers occupying most of the shifted quantum-confinement states between the band edge and those initially prepared during the photoexcitation. Similar data was obtained for the data collected with E_{exc} = 2.26 eV.

Spectra representing the occupancies of the charge carriers in the different, shifted quantum-confinement states as a function of time, $\Delta Abs_{Occ}(E, t)$, are determined by taking the difference between the QSR and TA spectra

$$\Delta Abs_{Occ}(E, t) = \Delta Abs_{QSR}(E, t) - \Delta Abs_{TA}(E, t) \quad (5)$$

The $\Delta Abs_{Occ}(E, t)$ for the CdTe QWs for t = 35 ps and 130 fs collected using E_{exc} = 2.75 eV are included in Figure 5b,d.

The full $\Delta Abs_{Occ}(E, t)$ data sets for E_{exc} = 2.75 and 2.26 eV, which reveal the occupancies of either electrons or holes in the different shifted, quantum-confinement features at all t, were obtained in a similar manner. As expected, at long t, e.g., at t = 35 ps, the $\Delta Abs_{Occ}(E, t)$ indicate the carriers were indeed predominantly in the lowest-energy states, near the band gap. In contrast, the $\Delta Abs_{Occ}(E, t)$ at short t, e.g., at t = 130 fs, contain numerous features associated with charge carriers occupying states throughout this spectral region just after photoexcitation, Figure 5d.

DISCUSSION

Ultimately, the dynamics of photogenerated electrons and holes as they relax to the band edge and then recombine as well as the energetics and trends of QSR of the different quantum-confinement states are important to investigate and characterize from nanomaterials and chemical physics perspectives. Comparison of the two-dimensional (2D) plots of the TA and the occupancy data collected for the CdTe QWs using E_{exc} = 2.75 eV, Figure 6, emphasizes how the QSR model permits the intraband relaxation dynamics to be extracted from the TA data. In Figure 6a, the $\Delta Abs_{TA}(E, t)$ are complicated

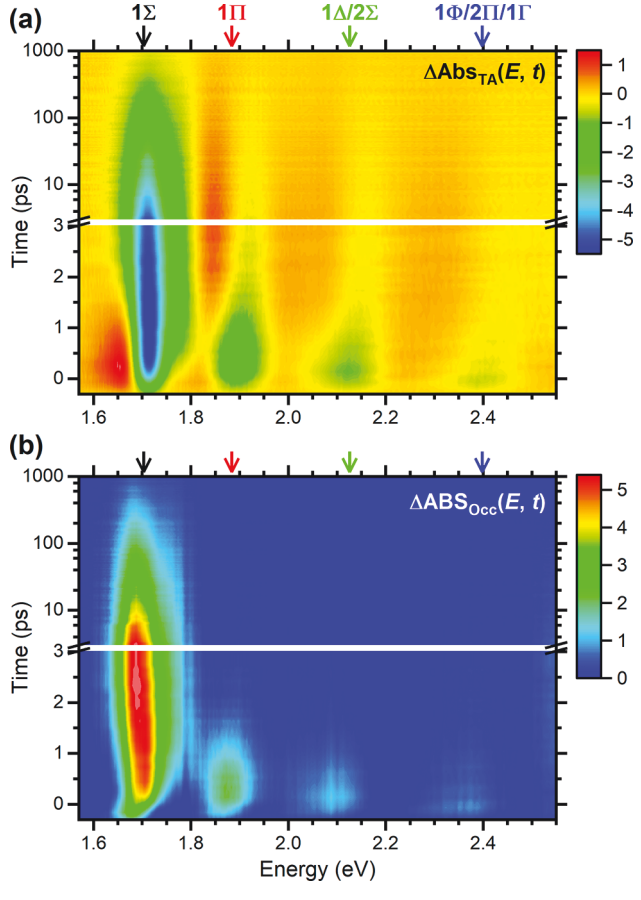

Figure 6. Comparison of the TA and occupancy data of CdTe QWs collected with E_{exc} = 2.75 eV. (a) The $\Delta Abs_{TA}(E, t)$ data contain overlapping induced-absorption and bleach signals that result in changes in peak positions with time and complicated dynamics. (b) The $\Delta Abs_{Occ}(E, t)$ data reveal the IRD of the charge carriers with time. The color scales in parts a and b are in mOD, and the arrows above each panel are the energies of the features identified in the steady-state absorption spectrum. The data in part b were published in a different format in ref 53.

https://dx.doi.org/10.1021/acs.jpcc.0c04755
J. Phys. Chem. C 2020, 124, 16702−16713

with overlapping induced-absorption (red) and bleach (green to blue) signals, and there is shifting of these features with t. Furthermore, the differential absorption signals at some energies switch from induced-absorption to bleach contributions, or vice versa, with t. In contrast, the $\Delta Abs_{Occ}(E, t)$ data, Figure 6b, are only associated with carriers in the different features, and they are much easier to interpret. It is particularly noteworthy that the amplitudes of the higher-energy $\Delta Abs_{Occ}(E, t)$ features associated with excited quantum-confinement states appear and decay away faster than the lower-energy features. This is consistent with the relaxation of the carriers from one state to the next until they reach the band edge. The carriers in the lowest-energy 1Σ states are then long-lived with lifetimes approaching nanoseconds. It is also revealed that the features at higher energies in the $\Delta Abs_{TA}(E, t)$ data are significantly longer lived than the corresponding features in the $\Delta Abs_{Occ}(E, t)$ data. These differences are directly attributed to the contributions from QSR that remain for as long as there are carriers in the QWs. A detailed description of the intraband relaxation dynamics of the charge carriers in the CdTe QWs is reported in ref 53.

The implementation of the QSR model on the TA data collected for the CdTe QWs using E_{exc} = 2.75 eV revealed there is an energetic shift of the higher-energy spectral features by $\Delta E_{QSR}(t)$ = 13.0(1.0) meV at long t, after the carriers relaxed to the 1Σ states at the band edge. The same shift of $\Delta E_{QSR}(t)$ = 12(2) meV was identified for the E_{exc} = 2.26 eV data. There is no *a priori* reasoning or justification for the different quantum-confinement states to experience uniform QSR. The peak energies for each of the features in the $\Delta Abs_{Occ}(E, t)$ were identified by fitting the spectrum at each t to a sum of Gaussians, one for each feature.

The temporal dependence of the energies of each feature in the $\Delta Abs_{Occ}(E, t)$ data collected with E_{exc} = 2.75 and 2.26 eV are plotted as filled symbols in Figure 7a and b, respectively. For comparison, the peak energies of the bleach features in the $\Delta Abs_{TA}(E, t)$ data are plotted as open symbols. The energies of the features present in the $Abs_{SS}(E)$ spectrum are indicated with vertical dashed lines. The $\Delta Abs_{Occ}(E, t)$ features are labeled with primes in Figure 7 to emphasize these states are shifted due to QSR, thus the lowest energy feature in the photoexcited CdTe QWs is the 1Σ′. The QSR shifts all of the features to lower energies with the largest shifts measured during the excitation pulse, −400 fs ≤ t ≤ 200 fs. Shifts as large as 71 meV below the steady-state energy were identified for the 1Δ′/2Σ′ feature in the E_{exc} = 2.75 eV data. The 1Σ′ occupancy feature for E_{exc} = 2.75 eV shifts from −25 to +3 meV within 600 fs and then to −17 meV on longer time scales after excitation. Similarly, shifts of up to 77 meV were identified for the 1Φ′/2Π′/1Γ′ feature in the E_{exc} = 2.26 eV data. Note that this excitation energy is not sufficient to populate the states within this feature since the 1Φ/2Π/1Γ feature in the $Abs_{SS}(E)$ spectrum is at 2.398 eV. Thus, these signals can only be associated with QSR of these states and not by occupancies in these excited levels. As reported elsewhere,[53] the fast shifting is due to contributions from the holes and the slower contributions are from the electrons sampling different quantum-confinement states while relaxing the band edge. These large shifts are not associated with the presence of multiple electron−hole pairs, as described above. It is also important to emphasize that the centers of the features in the TA spectra tend to shift to the opposite direction, toward higher transition energies than the steady-state features with t,

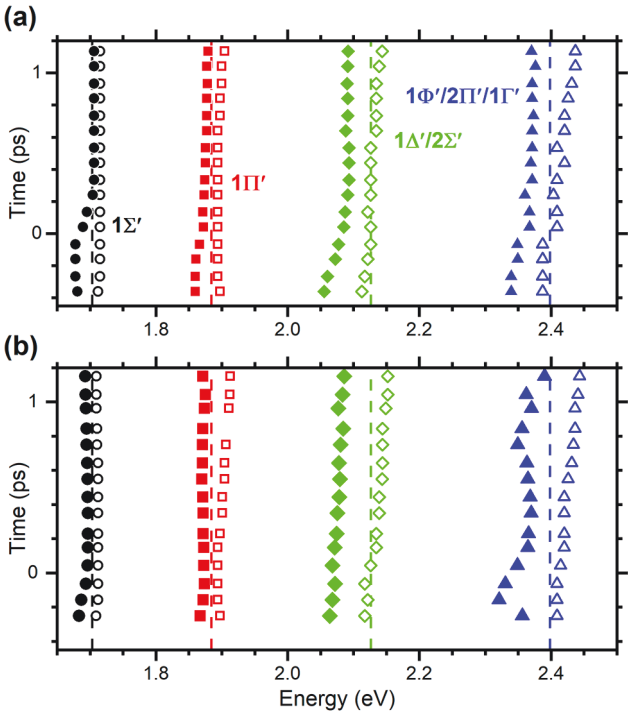

Figure 7. Comparison of peak energies in the $\Delta Abs_{Occ}(E, t)$ and $\Delta Abs_{TA}(E, t)$ data for CdTe QWs. (a and b) The energies of the features present in the $\Delta Abs_{TA}(E, t)$ spectra (open symbols) and in the $\Delta Abs_{Occ}(E, t)$ spectra (filled symbols) are plotted versus t for the data collected using E_{exc} = 2.75 and 2.26 eV are included in parts a and b, respectively. The dashed lines are the energies of the features identified in the steady-state absorption spectrum.

and the magnitudes of the shifts are less than those in the occupancy data.

The QSR of the quantum-confinement states of the CdTe QWs results in energetic shifts to lower energies upon photoexcitation. The energies of the different $\Delta Abs_{Occ}(E, t)$ features shift by varying amounts as the carriers relax to the band edge states. After the carriers reach the band-edge states, the energetic shift of each feature remains constant. The $\Delta Abs_{Occ}(E, t)$ spectrum near the 1Σ′ feature acquired at t = 35 ps and the $Abs_{SS}(E)$ spectrum are plotted as blue and black, respectively, in Figure 8 to emphasize the amount of this shift. We fit (gray) the $\Delta Abs_{Occ}(E, 35\ ps)$ occupancy spectrum in this low-energy region to a sum of two Gaussian peaks (yellow) to identify the energetic centers of the occupancy features. The higher-energy Gaussian is attributed to the 1Σ*′ transitions, and it is shifted by ∼14 meV to lower energy than the 1Σ* feature identified in the $Abs_{SS}(E)$ spectrum. The lower-energy Gaussian is attributed to the 1Σ′ transitions, and it is shifted by ∼17 meV to lower energy than the 1Σ absorption feature. The energy of the 1Σ′ feature is the same within error as the energy of the maximum of the $PL(E)$ spectrum (red; Figure 8). The breadths of the $PL(E)$ spectrum and the 1Σ′ Gaussian are similar, although there is a slight asymmetry in the $PL(E)$ spectrum with a tail extending to lower emission energies. We conclude that radiative recombination of electron/hole pairs occurs from the shifted quantum-confinement states associated with the 1Σ′ occupancy feature. Thus, the Stokes shift of the $PL(E)$ spectrum from the lowest-energy feature in the $Abs_{SS}(E)$ spectrum of these CdTe QWs is attributed to QSR, especially at the low excitation fluences

https://dx.doi.org/10.1021/acs.jpcc.0c04755
J. Phys. Chem. C 2020, 124, 16702−16713

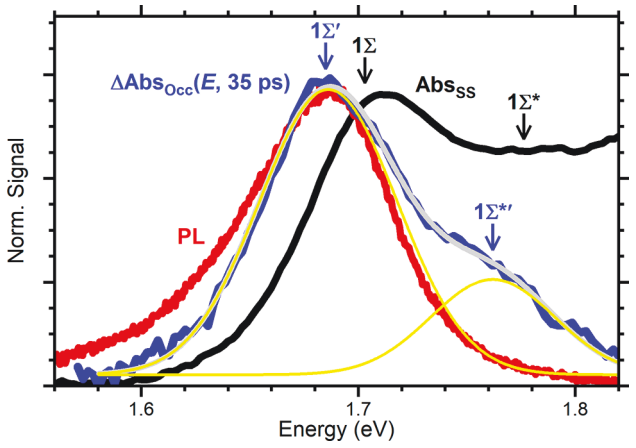

Figure 8. Comparison of 1Σ′ occupancy signal to the PL profile of the CdTe QWs. The $Abs_{SS}(E)$, $PL(E)$ (E_{Exc} = 2.76 eV), and $\Delta Abs_{Occ}(E,$ 35 ps) spectra were normalized to approximately the same maximum value and are plotted as black, red, and blue, respectively. The $\Delta Abs_{Occ}(E,$ 35 ps) spectrum was fit (gray) to a sum of two Gaussian peaks (yellow).

used in these experiments, and not to BGR,[77−82] Stark shifting of the quantum-confinement states,[1,28,43,49,83] or the stabilization of biexcitons.[1,3,25,27−30,32,33,43−45]

CONCLUSIONS

In summary, the QSR model presented here is associated with the energetic shifting of the quantum-confinement states in NPs that results from photoexcitation and the change in the electronic densities with the promotion of an electron to the CB and the formation of a hole in the VB. The steady-state absorption spectrum of the sample can be used to quantify the contributions from QSR that are present in TA data. Once the QSR contributions are identified and subtracted from the TA data, occupancy data, $\Delta Abs_{Occ}(E, t)$, are obtained that reveal those transitions that are bleached due to either electron or hole occupancies in the quantum-confinement states. The features within the $\Delta Abs_{Occ}(E, t)$ spectra enable the energetics of the quantum-confinement states to be tracked with time and the kinetics of the electrons and holes relaxing through these states to be mapped and characterized. The QSR of the lowest-energy states dictates the Stokes shift of the PL from the lowest-energy absorption feature for the CdTe QWs. This QSR model is not limited to CdTe QWs, and it should be a general phenomenon in NPs and large clusters and perhaps in other materials, such as carbon nanotubes. Samples with a large Stokes shift may be indicative of significant QSR.

ASSOCIATED CONTENT

Supporting Information

The Supporting Information is available free of charge at https://pubs.acs.org/doi/10.1021/acs.jpcc.0c04755.

Details of the synthesis of the CdTe QWs, steady-state optical spectroscopy, quantum-confinement state and transition strength calculations, transient absorption measurements, extraction of occupancy contributions, exponential fitting (PDF)

AUTHOR INFORMATION

Corresponding Author

Richard A. Loomis − *Department of Chemistry and Institute of Materials Science and Engineering, Washington University in Saint Louis, Saint Louis, Missouri 63130, United States;* orcid.org/0000-0002-3172-6336; Email: loomis@wustl.edu

Authors

William M. Sanderson − *Department of Chemistry and Institute of Materials Science and Engineering, Washington University in Saint Louis, Saint Louis, Missouri 63130, United States*

Joshua Schrier − *Department of Chemistry, Fordham University, The Bronx, New York 10458, United States;* orcid.org/0000-0002-2071-1657

Complete contact information is available at: https://pubs.acs.org/10.1021/acs.jpcc.0c04755

Notes

The authors declare no competing financial interest.

ACKNOWLEDGMENTS

This work was supported by the NSF under grants DMR-1611149 and DMR-1905751 (R.A.L.). J.S. acknowledges the Henry Dreyfus Teacher-Scholar Award (TH-14-010). This research used resources of the National Energy Research Scientific Computing Center (NERSC), a U.S. Department of Energy Office of Science User Facility operated under Contract No. DE-AC02-05CH11231. The authors are indebted to W.E. Buhro and F. Wang for making the CdTe QWs used in these studies.

REFERENCES

(1) Klimov, V. I.; McBranch, D. W.; Leatherdale, C. A.; Bawendi, M. G. Electron and Hole Relaxation Pathways in Semiconductor Quantum Dots. *Phys. Rev. B: Condens. Matter Mater. Phys.* **1999**, *60*, 13740−13749.

(2) Klimov, V. I.; Mikhailovsky, A. A.; McBranch, D. W.; Leatherdale, C. A.; Bawendi, M. G. Mechanisms for Intraband Energy Relaxation in Semiconductor Quantum Dots: The Role of Electron-Hole Interactions. *Phys. Rev. B: Condens. Matter Mater. Phys.* **2000**, *61*, R13349−R13352.

(3) Sewall, S. L.; Cooney, R. R.; Anderson, K. E. H.; Dias, E. A.; Kambhampati, P. State-to-State Exciton Dynamics in Semiconductor Quantum Dots. *Phys. Rev. B: Condens. Matter Mater. Phys.* **2006**, *74*, 235328.

(4) Knowles, K. E.; McArthur, E. A.; Weiss, E. A. A Multi-Timescale Map of Radiative and Nonradiative Decay Pathways for Excitons in CdSe Quantum Dots. *ACS Nano* **2011**, *5*, 2026−2035.

(5) Labrador, T.; Dukovic, G. Simultaneous Determination of Spectral Signatures and Decay Kinetics of Excited State Species in Semiconductor Nanocrystals Probed by Transient Absorption Spectroscopy. *J. Phys. Chem. C* **2020**, *124*, 8439−8447.

(6) Kirchhuebel, T.; Monti, O. L. A.; Munakata, T.; Kera, S.; Forker, R.; Fritz, T. The Role of Initial and Final States in Molecular Spectroscopies. *Phys. Chem. Chem. Phys.* **2019**, *21*, 12730−12747.

(7) Emin, D. *Polarons*; Cambridge University Press: New York, 2013; p 227.

(8) Landau, L. D.; Pekar, S. I. Effective Mass of a Polaron. *Ukr. J. Phys.* **2008**, *53*, 71−74.

(9) Chatterjee, A.; Mukhopadhyay, S. *Polarons and Bipolarons: An Introduction*; CRC Press, Taylor & Francis Group: Boca Raton, FL, 2019; p 464.

(10) Mears, A. L.; Stradling, R. A.; Inall, E. K. The Evidence for an Enhancement of the Polaron Effect Observed in Magnetophonon Resistance Oscillations in CdTe. *J. Phys. C: Solid State Phys.* **1968**, *1*, 821−826.
(11) Bajaj, K. K. Cyclotron Resonance of Polarons in CdTe. *Solid State Commun.* **1970**, *8*, 1907−1909.
(12) Helm, M.; Knap, W.; Seidenbusch, W.; Lassnig, R.; Gornik, E.; Triboulet, R.; Taylor, L. L. Polaron Cyclotron Resonance in *n*-CdTe and *n*-InP. *Solid State Commun.* **1985**, *53*, 547−550.
(13) Cohn, D. R.; Larsen, D. M.; Lax, B. Polaron Zeeman Effect in CdTe. *Phys. Rev. B* **1972**, *6*, 1367−1375.
(14) Sellami, K.; Jaziri, S. Exciton-Polaron in a CdSe Quantum Dot under an Applied Magnetic Field. *Phys. E* **2005**, *26*, 143−148.
(15) Rodina, A.; Efros, A. L. Magnetic Properties of Nonmagnetic Nanostructures: Dangling Bond Magnetic Polaron in CdSe Nanocrystals. *Nano Lett.* **2015**, *15*, 4214−4222.
(16) Sun, Z.; Swart, I.; Delerue, C.; Vanmaekelbergh, D.; Liljeroth, P. Orbital and Charge-Resolved Polaron States in CdSe Dots and Rods Probed by Scanning Tunneling Spectroscopy. *Phys. Rev. Lett.* **2009**, *102*, 196401.
(17) Prodanović, N.; Vukmirović, N.; Ikonić, Z.; Harrison, P.; Indjin, D. Importance of Polaronic Effects for Charge Transport in CdSe Quantum Dot Solids. *J. Phys. Chem. Lett.* **2014**, *5*, 1335−1340.
(18) Roy, K.; Nath, S.; Ghosh, N. K. Hole-Polarons and Bipolarons in the Holstein $t-J$ Model: Relevance of Inter-Site Hole-Phonon Interaction. *Phys. Lett. A* **2019**, *383*, 1510−1515.
(19) Yanar, S.; Sevim, A.; Boyacioglu, B.; Saglam, M.; Mukhopadhyaya, S.; Chatterjee, A. Polaronic Effects in a Gaussian Quantum Dot. *Superlattices Microstruct.* **2008**, *43*, 208−239.
(20) Mukhopadhyay, S.; Chatterjee, A. Polaronic Correction to the First Excited Electronic Energy Level in Semiconductor Quantum Dots with Parabolic Confinement. *Phys. Lett. A* **1998**, *240*, 100−104.
(21) Feng, D. H.; Xu, Z. Z.; Jia, T. Q.; Li, X. X.; Li, C. B.; Sun, H. Y.; Xu, S. Z. Polaronic Correction to the First Excited Electronic Energy Level in Ananisotropic Semiconductor Quantum Dot. *Eur. Phys. J. B* **2005**, *44*, 15−20.
(22) Kervan, N.; Altanhan, T.; Chatterjee, A. A Variational Approach with Squeezed-States for the Polaronic Effects in Quantum Dots. *Phys. Lett. A* **2003**, *315*, 280−287.
(23) Lampert, M. A. Mobile and Immobile Effective-Mass-Particle Complexes in Nonmetallic Solids. *Phys. Rev. Lett.* **1958**, *1*, 450−453.
(24) Kuwata-Gonokami, M. 2.07 - High-Density Excitons in Semiconductors. In *Comprehensive Semiconductor Science and Technology*, Bhattacharya, P.; Fornari, R.; Kamimura, H., Eds. Elsevier: Amsterdam, 2011; pp 213−255.
(25) Hu, Y. Z.; Koch, S. W.; Lindberg, M.; Peyghambarian, N.; Pollock, E. L.; Abraham, F. F. Biexcitons in Semiconductor Quantum Dots. *Phys. Rev. Lett.* **1990**, *64*, 1805−1807.
(26) Ikezawa, M.; Masumoto, Y.; Takagahara, T.; Nair, S. V. Biexciton and Triexciton States in Quantum Dots in the Weak Confinement Regime. *Phys. Rev. Lett.* **1997**, *79*, 3522−3525.
(27) Park, S. H.; Morgan, R. A.; Hu, Y. Z.; Lindberg, M.; Koch, S. W.; Peyghambarian, N. Nonlinear Optical Properties of Quantum-Confined CdSe Microcrystallites. *J. Opt. Soc. Am. B* **1990**, *7*, 2097−2105.
(28) Klimov, V.; Hunsche, S.; Kurz, H. Biexciton Effects in Femtosecond Nonlinear Transmission of Semiconductor Quantum Dots. *Phys. Rev. B: Condens. Matter Mater. Phys.* **1994**, *50*, 8110−8113.
(29) Kang, K. I.; Kepner, A. D.; Gaponenko, S. V.; Koch, S. W.; Hu, Y. Z.; Peyghambarian, N. Confinement-Enhanced Biexciton Binding Energy in Semiconductor Quantum Dots. *Phys. Rev. B: Condens. Matter Mater. Phys.* **1993**, *48*, 15449−15452.
(30) Schnitzenbaumer, K. J.; Labrador, T.; Dukovic, G. Impact of Chalcogenide Ligands on Excited State Dynamics in CdSe Quantum Dots. *J. Phys. Chem. C* **2015**, *119*, 13314−13324.
(31) Seiler, H.; Palato, S.; Sonnichsen, C.; Baker, H.; Kambhampati, P. Seeing Multiexcitons through Sample Inhomogeneity: Band-Edge Biexciton Structure in CdSe Nanocrystals Revealed by Two-Dimensional Electronic Spectroscopy. *Nano Lett.* **2018**, *18*, 2999−3006.
(32) Klimov, V. I. Properties of Multiexcitons in Semiconductor Nanocrystals. *Annu. Rev. Phys. Chem.* **2007**, *58*, 635−673.
(33) Yan, Y.; Chen, G.; Van Patten, P. G. Ultrafast Exciton Dynamics in CdTe Nanocrystals and Core/Shell CdTe/CdS Nanocrystals. *J. Phys. Chem. C* **2011**, *115*, 22717−22728.
(34) Sewall, S. L.; Franceschetti, A.; Cooney, R. R.; Zunger, A.; Kambhampati, P. Direct Obervation of the Structure of Band-Edge Biexcitons in Colloidal Semiconductor CdSe Quantum Dots. *Phys. Rev. B: Condens. Matter Mater. Phys.* **2009**, *80*, 081310.
(35) Sewall, S. L.; Cooney, R. R.; Dias, E. A.; Tyagi, P.; Kambhampati, P. State-Resolved Observation in Real Time of the Structural Dynamics of Multiexcitons in Semiconductor Nanocrystals. *Phys. Rev. B: Condens. Matter Mater. Phys.* **2011**, *84*, 235304.
(36) Baars, T.; Braun, W.; Bayer, M.; Forchel, A. Biexcitons in Semiconductor Quantum Wires. *Phys. Rev. B: Condens. Matter Mater. Phys.* **1998**, *58*, R1750−R1753.
(37) Crottini, A.; Staehli, J. L.; Deveaud, B.; Wang, X. L.; Ogura, M. One-Dimensional Biexcitons in a Single Quantum Wire. *Solid State Commun.* **2002**, *121*, 401−405.
(38) Wagner, H. P.; Tranitz, H.-P.; Langbein, W.; Hvam, J. M.; Bacher, G.; Forchel, A. Biexciton Binding Energy in ZnSe Quantum Wells and Quantum Wires. *Phys. Status Solidi B* **2002**, *231*, 11−18.
(39) Feltrin, A.; Michelini, F.; Staehli, J. L.; Deveaud, B.; Savona, V.; Toquant, J.; Wang, X. L.; Ogura, M. Localization-Dependent Photoluminescence Spectrum of Biexcitons in Semiconductor Quantum Wires. *Phys. Rev. Lett.* **2005**, *95*, 177404.
(40) Hayamizu, Y.; Yoshita, M.; Takahashi, Y.; Akiyama, H.; Ning, C. Z.; Pfeiffer, L. N.; West, K. W. Biexciton Gain and the Mott Transition in GaAs Quantum Wires. *Phys. Rev. Lett.* **2007**, *99*, 167403.
(41) Zhai, L.-X.; Wang, Y.; Miao, W.-D.; Liu, J.-J. The Binding Energy and Structure of Biexcitons in Quantum Wires. *J. Appl. Phys.* **2013**, *114*, 093702.
(42) Li, Q.; Lian, T. Area- and Thickness-Dependent Biexciton Auger Recombination in Colloidal CdSe Nanoplatelets: Breaking the "Universal Volume Scaling Law. *Nano Lett.* **2017**, *17*, 3152−3158.
(43) Morgan, D. P.; Maddux, C. J. A.; Kelley, D. F. Transient Absorption Spectroscopy of CdSe Nanoplatelets. *J. Phys. Chem. C* **2018**, *122*, 23772−23779.
(44) Li, Q.; Lian, T. A Model for Optical Gain in Colloidal Nanoplatelets. *Chem. Sci.* **2018**, *9*, 728−734.
(45) Hu, Y. Z.; Lindberg, M.; Koch, S. W. Theory of Optically Excited Intrinsic Semiconductor Quantum Dots. *Phys. Rev. B: Condens. Matter Mater. Phys.* **1990**, *42*, 1713−1723.
(46) Efros, A. L.; Rodina, A. V. Confined Excitons, Trions and Biexcitons in Semiconductor Microcrystals. *Solid State Commun.* **1989**, *72*, 645−649.
(47) Guyot-Sionnest, P.; Shim, M.; Matranga, C.; Hines, M. Intraband Relaxation in CdSe Quantum Dots. *Phys. Rev. B: Condens. Matter Mater. Phys.* **1999**, *60*, R2181.
(48) Puthussery, J.; Lan, A. D.; Kosel, T. H.; Kuno, M. Band-Filling of Solution-Synthesized CdS Nanowires. *ACS Nano* **2008**, *2*, 357−367.
(49) McArthur, E. A.; Morris-Cohen, A. J.; Knowles, K. E.; Weiss, E. A. Charge Carrier Resolved Relaxation of the First Excitonic State in CdSe Quantum Dots Probed with near-Infrared Transient Absorption Spectroscopy. *J. Phys. Chem. B* **2010**, *114*, 14514−14520.
(50) Peterson, M. D.; Cass, L. C.; Harris, R. D.; Edme, K.; Sung, K.; Weiss, E. A. The Role of Ligands in Determining the Exciton Relaxation Dynamics in Semiconductor Quantum Dots. *Annu. Rev. Phys. Chem.* **2014**, *65*, 317−339.
(51) Mooney, J.; Krause, M. M.; Kambhampati, P. Connecting the Dots: The Kinetics and Thermodynamics of Hot, Cold, and Surface-Trapped Excitons in Semiconductor Nanocrystals. *J. Phys. Chem. C* **2014**, *118*, 7730−7739.
(52) Robel, I.; Bunker, B. A.; Kamat, P. V.; Kuno, M. Exciton Recombination Dynamics in CdSe Nanowires: Bimolecular to Three-Carrier Auger Kinetics. *Nano Lett.* **2006**, *6*, 1344−1349.

https://dx.doi.org/10.1021/acs.jpcc.0c04755
J. Phys. Chem. C 2020, 124, 16702−16713

(53) Sanderson, W. M.; Schrier, J.; Wang, F.; Buhro, W. E.; Loomis, R. A. Intraband Relaxation Dynamics of Charge Carriers within CdTe Quantum Wires. *J. Phys. Chem. Lett.* **2020**, *11*, 4901−4910.
(54) Sun, J.; Wang, L. W.; Buhro, W. E. Synthesis of Cadmium Telluride Quantum Wires and the Similarity of Their Effective Band Gaps to Those of Equidiameter Cadmium Telluride Quantum Dots. *J. Am. Chem. Soc.* **2008**, *130*, 7997−8005.
(55) Liu, Y.-H.; Wang, F.; Hoy, J.; Wayman, V. L.; Steinberg, L. K.; Loomis, R. A.; Buhro, W. E. Bright Core−Shell Semiconductor Quantum Wires. *J. Am. Chem. Soc.* **2012**, *134*, 18797−18803.
(56) Li, J.; Wang, L.-W. Band-Structure-Corrected Local Density Approximation Study of Semiconductor Quantum Dots and Wires. *Phys. Rev. B: Condens. Matter Mater. Phys.* **2005**, *72*, 125325.
(57) Sun, J. W.; Buhro, W. E.; Wang, L. W.; Schrier, J. Electronic Structure and Spectroscopy of Cadmium Telluride Quantum Wires. *Nano Lett.* **2008**, *8*, 2913−2919.
(58) Wang, L.-W. *Computational Material Science and Nano Science Group*; Lawrence Berkeley National Laboratory. http://cmsn.lbl.gov/html/PEtot/PEtot.html (accessed February 3, 2019).
(59) Wang, L.-W. Charge-Density Patching Method for Unconventional Semiconductor Binary Systems. *Phys. Rev. Lett.* **2002**, *88*, 256402.
(60) Wang, L.-W. *Computational Material Science and Nano Science Group*; Lawrence Berkeley National Laboratory. http://cmsn.lbl.gov/html/Escan/DOE-nano/pescan.htm (accessed February 3, 2019).
(61) Schrier, J.; Demchenko, D. O.; Lin, W.; Alivisatos, A. P. Optical Properties of ZnO/ZnS and ZnO/ZnTe Heterostructures for Photovoltaic Applications. *Nano Lett.* **2007**, *7*, 2377−2382.
(62) Wang, L.-W. Calculating the Density of States and Optical-Absorption Spectra of Large Quantum Systems by the Plane-Wave Moments Method. *Phys. Rev. B: Condens. Matter Mater. Phys.* **1994**, *49*, 10154−10158.
(63) Guyot-Sionnest, P. Electrical Transport in Colloidal Quantum Dot Films. *J. Phys. Chem. Lett.* **2012**, *3*, 1169−1175.
(64) Guyot-Sionnest, P.; Wehrenberg, B.; Yu, D. Intraband Relaxation in CdSe Nanocrystals and the Strong Influence of the Surface Ligands. *J. Chem. Phys.* **2005**, *123*, 074709.
(65) Morgan, D.; Kelley, D. F. Role of Surface States in Silver-Doped Cdse and CdSe/CdS Quantum Dots. *J. Phys. Chem. C* **2018**, *122*, 10627−10636.
(66) Griffin, G. B.; Ithurria, S.; Dolzhnikov, D. S.; Linkin, A.; Talapin, D. V.; Engel, G. S. Two-Dimensional Electronic Spectroscopy of CdSe Nanoparticles at Very Low Pulse Power. *J. Chem. Phys.* **2013**, *138*, 014705.
(67) Sippel, P.; Albrecht, W.; van der Bok, J. C.; Van Dijk-Moes, R. J. A.; Hannappel, T.; Eichberger, R.; Vanmaekelbergh, D. Femtosecond Cooling of Hot Electrons in CdSe Quantum-Well Platelets. *Nano Lett.* **2015**, *15*, 2409−2416.
(68) Achtstein, A. W.; et al. *P*-State Luminescence in CdSe Nanoplatelets: Role of Lateral Confinement and a Longitudinal Optical Phonon Bottleneck. *Phys. Rev. Lett.* **2016**, *116*, 116802.
(69) Okuhata, T.; Tamai, N. Face-Dependent Electron Transfer in CdSe Nanoplatelet−Methyl Viologen Complexes. *J. Phys. Chem. C* **2016**, *120*, 17052−17059.
(70) Dong, S.; Pal, S.; Lian, J.; Chan, Y.; Prezhdo, O. V.; Loh, Z.-H. Sub-Picosecond Auger-Mediated Hole-Trapping Dynamics in Colloidal CdSe/CdS Core/Shell Nanoplatelets. *ACS Nano* **2016**, *10*, 9370−9378.
(71) Rabouw, F. T.; van der Bok, J. C.; Spinicelli, P.; Mahler, B.; Nasilowski, M.; Pedetti, S.; Dubertret, B.; Vanmaekelbergh, D. Temporary Charge Carrier Separation Dominates the Photoluminescence Decay Dynamics of Colloidal CdSe Nanoplatelets. *Nano Lett.* **2016**, *16*, 2047−2053.
(72) Diroll, B. T.; Fedin, I.; Darancet, P.; Talapin, D. V.; Schaller, R. D. Surface-Area-Dependent Electron Transfer between Isoenergetic 2D Quantum Wells and a Molecular Acceptor. *J. Am. Chem. Soc.* **2016**, *138*, 11109−11112.
(73) Cassette, E.; Pedetti, S.; Mahler, B.; Ithurria, S.; Dubertret, B.; Scholes, G. D. Ultrafast Exciton Dynamics in 2D in-Plane Heterostructures: Delocalization and Charge Transfer. *Phys. Chem. Chem. Phys.* **2017**, *19*, 8373−8379.
(74) Glennon, J. J.; Tang, R.; Buhro, W. E.; Loomis, R. A.; Bussian, D. A.; Htoon, H.; Klimov, V. I. Exciton Localization and Migration in Individual CdSe Quantum Wires at Low Temperatures. *Phys. Rev. B: Condens. Matter Mater. Phys.* **2009**, *80*, 081303.
(75) Carey, C. R.; Yu, Y.; Kuno, M.; Hartland, G. V. Ultrafast Transient Absorption Measurements of Charge Carrier Dynamics in Single II−VI Nanowires. *J. Phys. Chem. C* **2009**, *113*, 19077−19081.
(76) Vietmeyer, F.; Frantsuzov, P. A.; Janko, B.; Kuno, M. Carrier Recombination Dynamics in Individual CdSe Nanowires. *Phys. Rev. B: Condens. Matter Mater. Phys.* **2011**, *83*, 115319.
(77) Vashishta, P.; Kalia, R. K. Universal Behavior of Exchange-Correlation Energy in Electron-Hole Liquid. *Phys. Rev. B: Condens. Matter Mater. Phys.* **1982**, *25*, 6492−6495.
(78) Wegscheider, W.; Pfeiffer, L. N.; Dignam, M. M.; Pinczuk, A.; West, K. W.; McCall, S. L.; Hull, R. Lasing from Excitons in Quantum Wires. *Phys. Rev. Lett.* **1993**, *71*, 4071−4074.
(79) Cingolani, R.; Rinaldi, R.; Ferrara, M.; La Rocca, G. C.; Lage, H.; Heitmann, D.; Ploog, K.; Kalt, H. Band-Gap Renormalization in Quantum Wires. *Phys. Rev. B: Condens. Matter Mater. Phys.* **1993**, *48*, 14331−14337.
(80) Wang, K. H.; Bayer, M.; Forchel, A.; Ils, P.; Benner, S.; Haug, H.; Pagnod-Rossiaux, P.; Goldstein, L. Subband Renormalization in Dense Electron-Hole Plasmas in $In_{0.53}Ga_{0.47}As$/InP Quantum Wires. *Phys. Rev. B: Condens. Matter Mater. Phys.* **1996**, *53*, R10505.
(81) Titova, L. V.; et al. Dynamics of Strongly Degenerate Electron-Hole Plasmas and Excitons in Single InP Nanowires. *Nano Lett.* **2007**, *7*, 3383−3387.
(82) Perera, S.; et al. Nearly Intrinsic Exciton Lifetimes in Single Twin-Free GaAs/AlGaAs Core-Shell Nanowire Heterostructures. *Appl. Phys. Lett.* **2008**, *93*, 053110.
(83) Vietmeyer, F.; Chatterjee, R.; McDonald, M. P.; Kuno, M. Concerted Single-Nanowire Absorption and Emission Spectroscopy: Explaining the Origin of the Size-Dependent Stokes Shift in Single Cadmium Selenide Nanowires. *Phys. Rev. B: Condens. Matter Mater. Phys.* **2015**, *91*, 085422.
(84) Klimov, V. I.; McBranch, D. W. Auger-Process-Induced Charge Separation in Semiconductor Nanocrystals. *Phys. Rev. B: Condens. Matter Mater. Phys.* **1997**, *55*, 13173−13179.
(85) Klimov, V. I.; Mikhailovsky, A. A.; McBranch, D. W.; Leatherdale, C. A.; Bawendi, M. G. Quantization of Multiparticle Auger Rates in Semiconductor Quantum Dots. *Science* **2000**, *287*, 1011−1013.
(86) Htoon, H.; Hollingsworth, J. A.; Dickerson, R.; Klimov, V. I. Effect of Zero- to One-Dimensional Transformation on Multiparticle Auger Recombination in Semiconductor Quantum Rods. *Phys. Rev. Lett.* **2003**, *91*, 227401.
(87) Styers-Barnett, D. J.; Ellison, S. P.; Mehl, B. P.; Westlake, B. C.; House, R. L.; Park, C.; Wise, K. E.; Papanikolas, J. M. Exciton Dynamics and Biexciton Formation in Single-Walled Carbon Nanotubes Studied with Femtosecond Transient Absorption Spectroscopy. *J. Phys. Chem. C* **2008**, *112*, 4507−4516.
(88) Soavi, G.; Scotognella, F.; Brida, D.; Hefner, T.; Späth, F.; Antognazza, M. R.; Hertel, T.; Lanzani, G.; Cerullo, G. Ultrafast Charge Photogeneration in Semiconducting Carbon Nanotubes. *J. Phys. Chem. C* **2013**, *117*, 10849−10855.

https://dx.doi.org/10.1021/acs.jpcc.0c04755
J. Phys. Chem. C 2020, 124, 16702−16713